Maximum Power Point Estimation Based on Operating Conditions Classification for Photovoltaic Systems: A Case Study for Partial Shading

U.C. Turhal* and Y. Onal

Department of Electrical and Electronics Engineering, Bilecik Seyh Edebali University, Fatih Sultan Mehmet Bulvarı No:27, 11000, Bilecik, Turkey

Received: 22.02.2022 & Accepted: 31.05.2022

Doi: 10.12693/APhysPolA.142.256 *e-mail: ucigdem.turhal@bilecik.edu.tr

As a kind of operating condition, partial shading fault is an unavoidable occurrence in photovoltaic power generation, causing variations in the photovoltaic system's output power, panel current–voltage data, and power–voltage data, thus changing the maximum power point. The maximum power point information and the operating condition have to be known in order to make an accurate analysis and also increase the system safety, production, efficiency, and availability due to these variations during the analysis. In this paper, a novel customized maximum power point estimation method is proposed to detect the maximum voltage using a different operating condition classification system based on the common vector approach. Operating conditions consist of a standard test and three different types of partial shading, and 100% accuracy in classification is achieved. Then, the support vector regression is employed for the maximum voltage estimation in the classified operation condition. The data set used was obtained from the PSIM package simulation of a 250 W photovoltaic system under different studying conditions. The experimental results show that the proposed estimation method significantly reduces estimation errors and outperforms conventional voltage estimation at the maximum power point.

topics: maximum power point estimation, operating condition classification, common vector approach, support vector regression

1. Introduction

Solar energy (SE), one of the renewable energy resources, has some important properties such as environmental effects, sustainability, and low raw material cost. Therefore, SE comes to the forefront among fossil fuels and other renewable energy sources [1]. Conversion of SE into electrical energy is accomplished by serial and parallel connection of environmentally friendly, highly secure, clean, noiseless, and low maintenance requiring photovoltaic (PV) panels [2].

The power produced in PV panels is greatly affected by environmental factors, which customize the operating conditions (OC). These factors are the amount of solar irradiation (G), wind speed, ambient temperature, and panel temperature [3]. Due to these factors, the relationship between the power and voltage obtained at the output of the PV panel is nonlinear, and the position of the maximum power point (MPP) is variable [4]. However, different OC due to variable environmental effects cause the power at the system output to vary. In this case, MPP tracker (MPPT) methods are applied to integrate PV systems into the power grid and increase the efficiency of the PV system [5]. Thus, it is ensured that maximum power is obtained from the PV system, independent of the OC.

Although there are many MPPT applications in the literature, existing MPPT methods need to be developed to optimize the performance of PV systems [6–11]. This variation in MPP concludes that the methods of MPPT are highly dependent on different OCs [12]. Therefore, the MPPT method has to be customized based on the OC classification (OCC) for any particular PV system. One way to customize the MPPT method is the OCC based on the historical data of the PV system [13, 14]. In the literature, it is possible to come across studies in which the OCC is performed automatically according to historical data with various machine learning (ML) methods [15, 16]. In addition, it has been shown in various studies that this automatic classification with ML methods is faster and more effective than conventional manual classification [17–19].

In recent years, MPP estimation (MPPE) methods using ML algorithms have also become popular in addition to the commonly used MPPT methods. In MPPE methods, a function is determined using the historical data and the mathematical connection to calculate the maximum voltage and power data in the MPP. In general, the mathematical connection is established based on OCC [20]. Most current MPPE methods are based on current–voltage (I–V) curves in uniform solar irradiation, so many of these methods in the literature are applicable only in the case of uniform irradiation [21]. Thus, it is necessary to use regression or estimation models which assume that all input properties are not the same and are not independently distributed in the I–V curves obtained at different OC.

In this study, a novel customized MPP estimation method based on automatic OCC as different partial shading conditions (PSC) is proposed. In the case of PSC, the power–voltage (P–V) curves have multiple peaks, and only one of them is the global MPP (GMPP), while the others are local MPPs. The GMPP cannot be detected using conventional MPPT methods. The proposed MPPE method aims to detect GMPP by OCC with a minimum error rate and then apply the ML algorithm to the available historical data. In order to do the OCC automatically, the historical data measured for the PV system is used. The classification is performed by a supervised ML algorithm called the common vector approach (CVA) used in sufficient data cases [22]. After the OCC, the MPP voltage estimation at MPP is performed using the support vector regression (SVR) algorithm, which shows that the P–V curves have multiple peaks [23, 24]. The proposed method's performance is compared with other similar studies in order to show how small the modeling errors are. So, the OCC performance of the proposed method is compared with principal component analysis (PCA) used in a similar study in the literature, and the voltage estimation performance is compared with SVR without an OCC step and artificial neural networks (ANN). According to the experimental studies, the OCC before the voltage estimation at MPP significantly reduces the error rates in estimation. The contributions of the proposed method can be summarized as follows:

- Common vector approach is used for the OCC in the PV system for the first time in the literature.
- Detection of the PSC is performed without using irradiation sensors.
- Common vector approach and SVR are used together to solve the MPPE problem for the first time in the literature.
- For the estimation process where the I–V curve of the PV system is used, no additional equipment is required, so the method is cost-effective and also time-effective.

TABLE I

FL60-250MBP PV panel parameters.

PV panel parameter	Value
maximum power, P_{mmp}	250 W
current in MPP, I_{MPP}	8.21 A
voltage in MPP, V_{MPP}	30.52 V
short-circuit current, I_{sc}	8.64 A
open-circuit voltage, V_{oc}	37.67 V

The article is organized as follows: the PV system simulation model and the data obtained from these simulations are given in Sect. 2; the OCC, voltage estimation, and the experimental results of these processes are given in Sect. 3; conclusions are given in Sect. 4.

2. Description of the data set

In the study, two machine learning algorithms, the CVA classification algorithm and the SVR regression algorithm, were used for the proposed customized MPPE method. CVA method is an effective algorithm that reveals the common and unique properties that best describe an object class. SVR is a regression algorithm that is successfully used in nonlinear regression problems. The CVA for the OCC and SVR for MPPE were used together in this study.

2.1. Data acquisition

In this study, the PSIM package program, which provides fast and accurate results in the design, simulation, control, and analog and digital motor control of power electronics circuits, was used. In the case studies, the monocrystalline silicon FL60-250MBP photovoltaic panel was used. The main parameters of the PV panel used in the standard test conditions (STC) corresponding to 1000 W/m^2 solar irradiation and 25°C panel temperature and defined as healthy conditions are given in Table I [16].

To use the physical model of the PV panel, many parameter inputs are required. Some parameters can be obtained from manufacturers' datasheets, while other parameters need to be calculated. This model also takes into account the variation in light irradiance level and ambient temperature. The tested PV panel consists of 60 PV cells connected in series. Simulation tests were performed under STC and three different PSCs. PV panels are connected in series to increase the voltage. In simulations, each I–V feature is acquired over a one-minute period. Therefore, during 18 minutes, 18 different I–V curves are obtained for different temperatures (T) and solar irradiations (G) for 18 samples (S) in each condition. For STC and each PSC, there are generated 18 different I–V curves, each consisting of 2000 points, resulting in a total of 72 different I–V curves. A dataset containing 72 MPPs representing

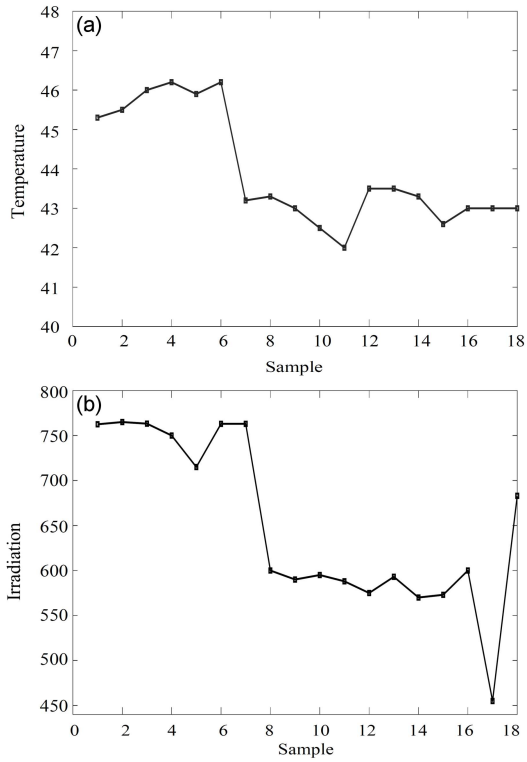

Fig. 1. (a) Different temperature (T) values and (b) different solar irradiation (G) values for 18 samples (S) in the STC.

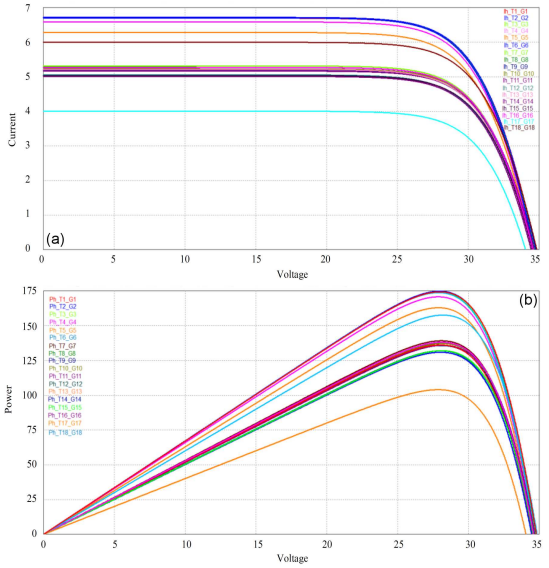

Fig. 2. Obtained (a) the current–voltage (I–V) and (b) the power–voltage (P–V) curves for a STC.

TABLE II

Maximum variation values of irradiance and temperature.

Partial shading condition	Max. temperature fluctuation [%]	Max. irradiation fluctuation [%]
PSC1	19.29%	48.01%
PSC2	12.20%	67.92%
PSC3	4.08%	40.00%

the four OCs of the PV panel is created. In Fig. 1, 18 different T values and 18 different G values applied to the PV panel in the STC are given.

When the values given in Fig. 1 are applied to the PV panel in the STC, the I–V and P–V curves obtained from the PV panel are shown in Fig. 2. Here, the Ih_T1_G1 curve is the current–voltage curve obtained by applying the $T1$ temperature $G1$ irradiation values to the PV panel in the case of STC. In addition, the Ph_T1_G1 curve is the power–voltage curve obtained by applying the $T1$ temperature $G1$ irradiation values to the PV panel in the case of STC. Maximum power fluctuates between 131.98 and 176.21 W due to $\max G$ fluctuation of 40.5% and $\max T$ fluctuation of 9.09%.

PSC is very common in PV systems installed in urban areas. PSC can be caused by passing clouds, nearby trees, and other buildings. In PSC, when the entire PV array receives non-uniform irradiation, the shaded PV cells absorb the electrical power produced by the unshaded cells, leading to hot spots that can irreversibly damage the panel. Module irregularities, such as the presence of cracks in one or more panels of the PV system, also lead to multiple peak P–V characteristic curves. To prevent this, bypass diodes are placed parallel to the panels. Bypass diodes used in PSC cause the maximum power to drop. Thanks to the global MPPE methods in the literature (e.g., [20]), maximum efficiency is obtained in PV panel systems. When the PV panel operates in STC, only one maximum peak occurs. However, one global peak occurs within the multiple local peaks in the case of PSC. PSC does not create a significant temperature difference between shaded and insulated panels, and all panels are considered to operate at the same temperature.

In the study, three different PSCs were applied, and in each of them, 18 temperature and 18 irradiation values were applied in turn, giving a total of 54 temperature and irradiation values applied for three PSCs. A value of 54 MPP was obtained. Of the first sub-string of the PV panel, 12 cells were partially shaded in PSC1. In PSC2, 12 cells of the first sub-string and 6 cells of the second sub-string, 18 cells in total, were partially shaded. One cell of the first sub-string and one cell of the third sub-string, 2 cells in total, were partially shaded in PSC3. Table II gives the maximum variation of irradiation and temperature values for PSC1, PSC2, and PSC3.

In Fig. 3, 18 different T and 18 different G values applied to the PV panel in the PSC1 are given. The values given in Fig. 3 have been applied to the PV panel in the PSC1 — the I–V and P–V curves obtained from the PV panel are shown

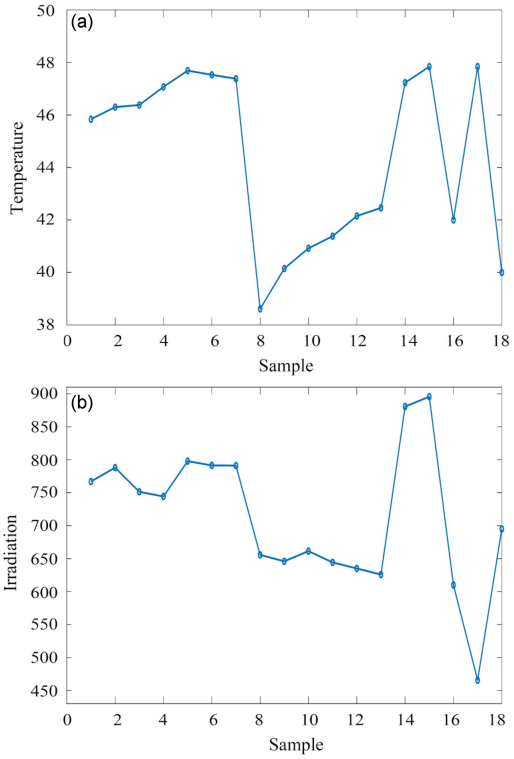

Fig. 3. (a) PV panel temperature and (b) solar irradiation values for the PSC1.

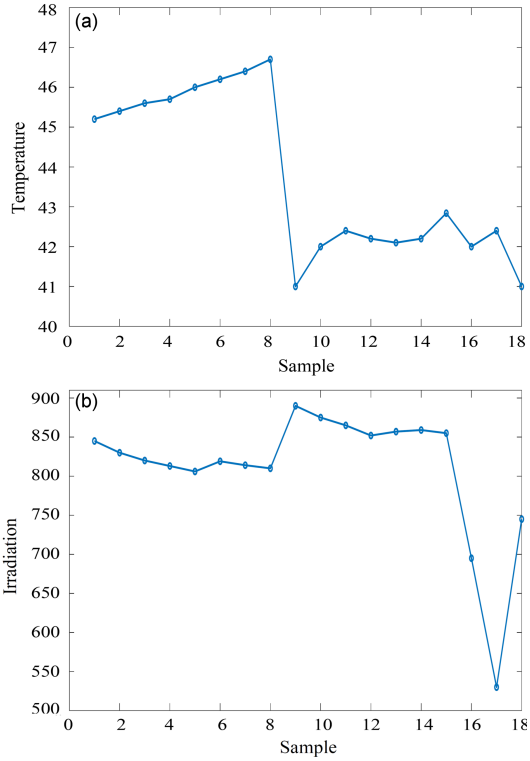

Fig. 5. (a) PV panel temperature and (b) solar irradiation values for the PSC2.

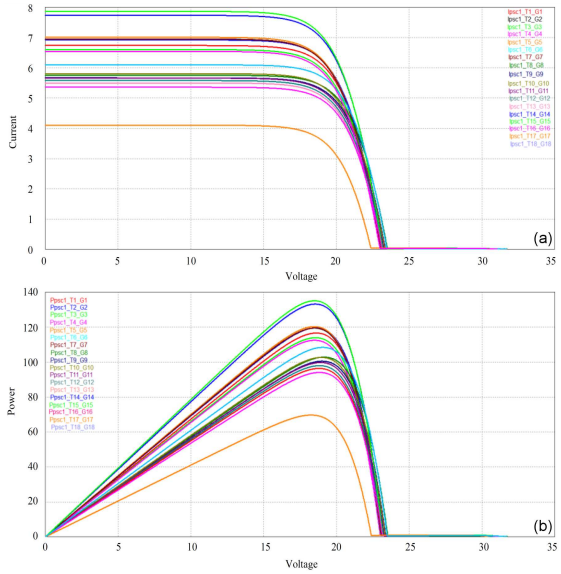

Fig. 4. Obtained (a) the current–voltage and (b) the power–voltage curves for the PSC1.

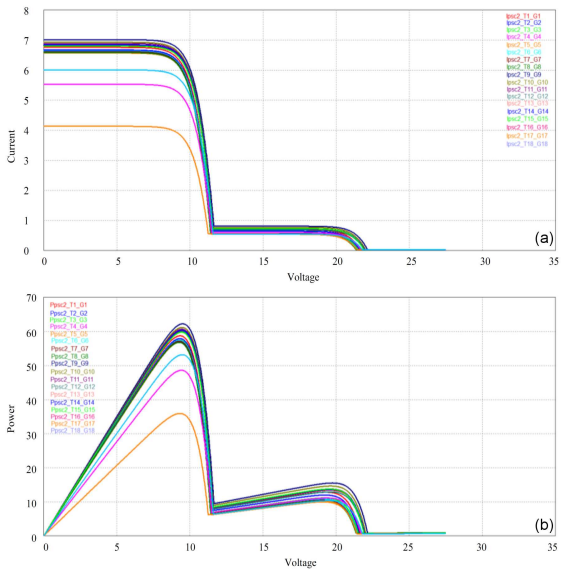

Fig. 6. Obtained (a) the current–voltage and (b) the power–voltage curves for the PSC2.

in Fig. 4. Here, the $\text{Ipsc}_1\_\text{T1}\_\text{G1}$ curve is the current–voltage curve obtained by applying the $T1$ temperature $G1$ irradiation values to the PV panel in the case of PSC1. In addition, the $\text{Ppsc}_1\_\text{T1}\_\text{G1}$ curve is the power–voltage curve obtained by applying the $T1$ temperature $G1$ irradiation values to the PV panel in the case of PSC1.

In Fig. 5, 18 different T and 18 different G values applied to the PV panel in the PSC2 are given. The values given in Fig. 5 have been applied to the PV panel in the PSC2 — the I–V and P–V curves obtained from the PV panel are shown in Fig. 6. Here, the $\text{Ipsc}_2\_\text{T1}\_\text{G1}$ curve is the current–voltage curve obtained by applying the $T1$

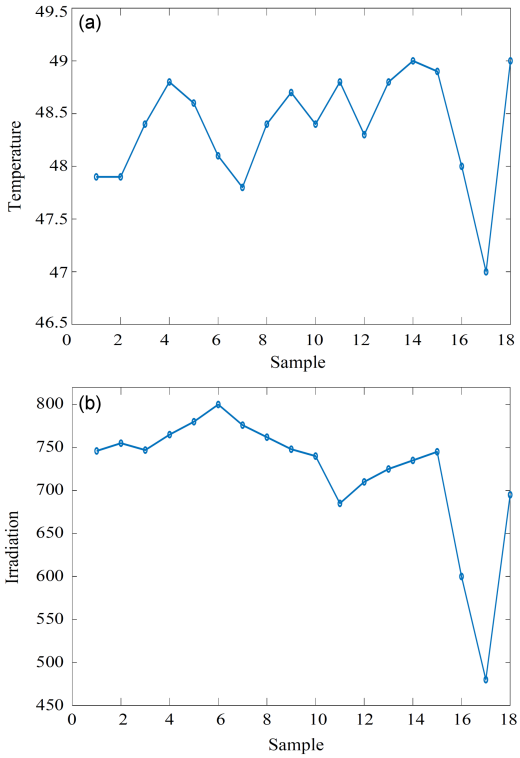

Fig. 7. (a) PV panel temperature and (b) solar irradiation values for the PSC3.

temperature $G1$ irradiation values to the PV panel in the case of PSC2. Also, the $\mathrm{Ppsc}_2\_\mathrm{T1}\_\mathrm{G1}$ curve is the power–voltage curve obtained by applying the $T1$ temperature $G1$ irradiation values to the PV panel in the case of PSC2.

In Fig. 7, 18 different T and 18 different G values applied to the PV panel in the PSC3 are given. The values given in Fig. 7 have been applied to the PV panel in the PSC3 — the I–V and P–V curves obtained from the PV panel are shown in Fig. 8. Here, the $\mathrm{Ipsc}_3\_\mathrm{T1}\_\mathrm{G1}$ curve is the current–voltage curve obtained by applying the $T1$ temperature $G1$ irradiation values to the PV panel in the case of PSC3. Also, the $\mathrm{Ppsc}_3\_\mathrm{T1}\_\mathrm{G1}$ curve is the power–voltage curve obtained by applying the $T1$ temperature $G1$ irradiation values to the PV panel in the case of PSC3.

2.2. Simulation model for customized MPPE method based on OCC

The simulation model consists of a PV panel, smart MPP estimator, direct current-to-direct current (DC-DC) boost converter, and a resistive load, as shown in Fig. 9. The PV panel consists of 3 sub-arrays of 20 cells connected in series and 3 parallel bypass diodes protecting each sub-array. The sampling period considered is equal to 5 μs. The proposed customized MPP estimator based on OCC provides a reference voltage, V_{MPP}. The error signal is obtained by comparing the maximum

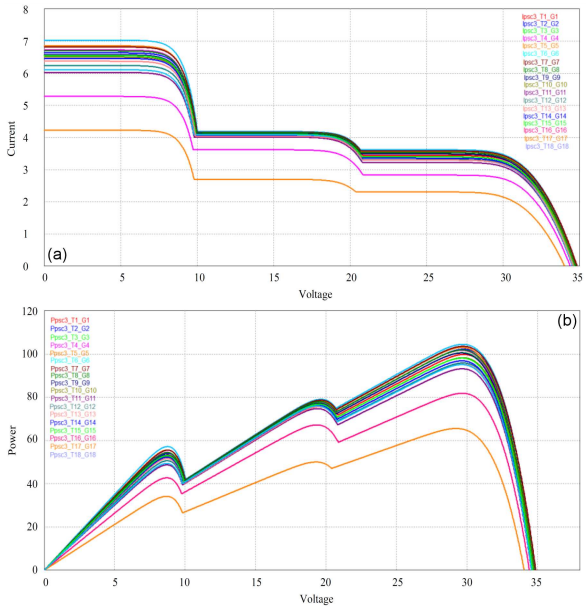

Fig. 8. Obtained (a) the current–voltage and (b) the power–voltage curves for the PSC3.

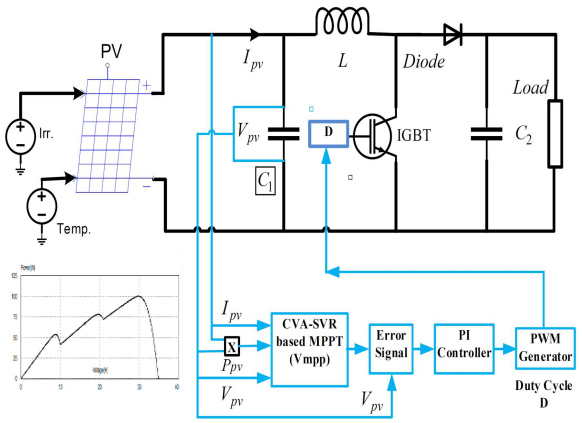

Fig. 9. The block diagram of OCC based voltage estimation at MPP in PV system with the DC–DC boost converter.

voltage with the voltage of the PV panel, V_{PV}. The obtained error signal is sent to the PI controller to generate control signals. The pulse width modulation signals of active switches are obtained by comparing the obtained control signal with the triangle signal. The OC of the PV panel is adjusted by controlling the output signal of the DC-DC) converter using pulse width modulation signals.

3. Customized MPPE based on OCC System

The overall flowchart of the proposed method including OCC and MPPE system is shown in Fig. 10.

3.1. Operating condition classification

In this paper, in order to perform automatic OCC by a supervised learning algorithm, CVA in sufficient data case is used. The feature space is decomposed into two subspaces, the range space, which is called the difference subspace (B), and the null space, called the indifference subspace, which is the orthogonal complement of B ($B^{\perp}$) in CVA. This method is used in problems such as multi-frame super-resolution of images [25], agricultural yield detection [26], power system fault detection [27], and photovoltaic fault detection [22]. The main goal in CVA is to find a unique common vector that preserves the inherent properties of a class. The algorithm is applied separately for each class, and a common vector is obtained for each class, where only the data of that class is used. This vector best expresses the common aspects of the data of that class.

The algorithm can be implemented as follows:

1. In the training phase for each class c ($c = 1, \ldots, C$ where C is the total class number), the within-class covariance matrices (S_W^c) are obtained as

$$S_W^c = \frac{1}{m}\sum_{j=1}^{m}(\boldsymbol{x}_j^c - \overline{\boldsymbol{x}}^c)(\boldsymbol{x}_j^c - \overline{\boldsymbol{x}}^c)^{\mathrm{T}}, \tag{1}$$

where $\overline{\boldsymbol{x}}^c = \frac{1}{m}\sum_{j=1}^{m}\boldsymbol{x}_j^c$ is the mean vector of class c and m is the number of sample in a class.

2 Eigen decomposition is applied to the covariance matrices given in (1). Then, the feature space composed of the two subspaces is obtained for each class. In this feature space, the eigenvectors to which the eigenvalues are corresponding, the smallest ones nearly close to zero, span the indifference subspace. These eigenvectors are used for feature extraction.

3 A common vector for each class is obtained by projecting the mean vector onto the indifference subspace as

$$\boldsymbol{x}_{\mathrm{com}}^c = \overline{\boldsymbol{x}}^c\, E^c, \quad E^c = \begin{Bmatrix} \uparrow & \vdots & \uparrow \\ e_1^{\mathrm{c}} & \vdots & e_k^{\mathrm{c}} \\ \downarrow & \vdots & \downarrow \end{Bmatrix}, \tag{2}$$

where k denotes the indices of the eigenvectors which span the indifference feature subspace of the c-th class covariance matrix.

4 In the test phase, the data ($\boldsymbol{x}_{\mathrm{test}}$) which will be classified is projected onto the indifference subspaces of all of the classes one by one, and a remaining vector ($\boldsymbol{x}_{\mathrm{test,\,rem}}^{\mathrm{c}}$) for the test data is obtained in each class, i.e.,

$$\boldsymbol{x}_{\mathrm{test,\,rem}}^c = \boldsymbol{x}_{\mathrm{test}} E^c. \tag{3}$$

Then, the distances between the class common vectors and the remaining vector of the test data in each class are computed as

$$\mathrm{class} = \arg\min_{1\le \mathrm{c} \le \mathrm{C}} \left|\left| \boldsymbol{x}_{\mathrm{test,\,rem}}^{\mathrm{c}} - \boldsymbol{x}_{\mathrm{com}}^c \right|\right|^2. \tag{4}$$

And the data is assigned to the class which the distance is min.

The proposed novel supervised OCC method that uses CVA is given in Fig. 11. The original dataset contains I, V, and P values measured at MPP of four different OCS, designated as one STC and three different PSCs. Data are measured for each OC for 18 min for different PV temperatures and different solar irradiation. Thus, 72 I–V and 72 P–V curves are obtained for four OCs in total. The MPP coordinates of each of these 72 curves are extracted using the PSIM SIMVIEW model. The I, V, and P (power) values at the global MPP for each of the I–V and P–V curves are used for the classification of the PV faults corresponding to the OC. An object from this dataset has a 1×3 dimensional vector form. The original dataset is partitioned into two sets, the training set, and the test set, using k-fold cross validation at the beginning of the classification system. In the proposed method, the k value is taken as 10. While the training set contains I, V, P data samples at MPP for specified OC, the test dataset contains data samples of which the OCs are not exact. By applying CVA to the training dataset, a common vector best describing OC is obtained and used for the OCC in the testing process.

In this OCC model, the data is very sensitive to changes in temperature and irradiation. Thus, it is hard to distinguish and classify different OCs, such as STC and different PSC. In this study, for the first time in the literature, an OCC model that applies CVA for extracting features and performs classification on the data obtained from MPPs is proposed. In the OCC model using CVA, 100% classification accuracy is achieved both in the training process and in the testing process in the OCC. The confusion matrices for both the training dataset and the test dataset are also given in Fig. 12.

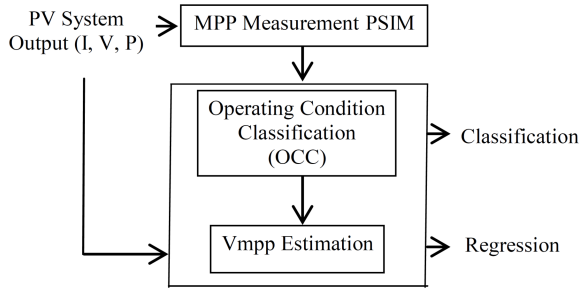

Fig. 10. Overall flowchart of the proposed customized MPP estimation method based on OCC system.

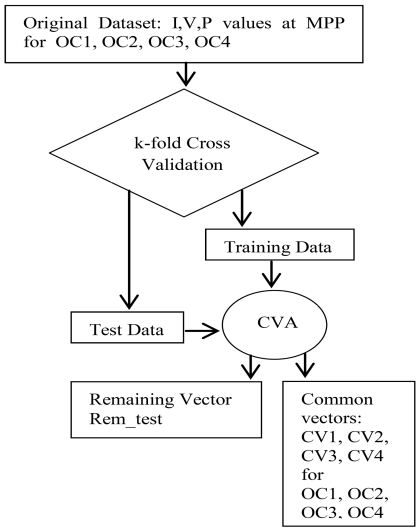

Fig. 11. The OCC process of a PV panel by applying CVA.

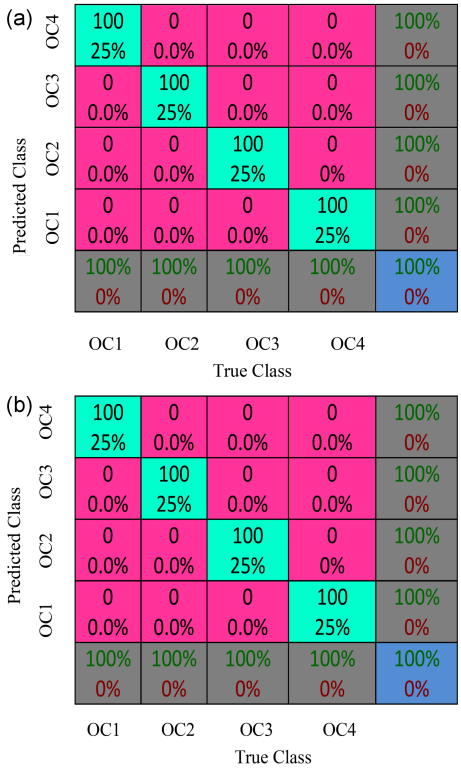

Fig. 12. Confusion matrices for (a) the test dataset, (b) the training dataset.

Data projections on the CVA feature subspace of the test dataset and of the training dataset can be seen in Figs. 13 and 14, respectively. As can be seen in Fig. 13, the proposed MPPE method can entirely distinguish the OC accurately.

In the case of partial shading diagnosis, the OCC results obtained with CVA and PCA through the analysis of the maximum power point (MPP) coordinates are both 100%. However, Table III

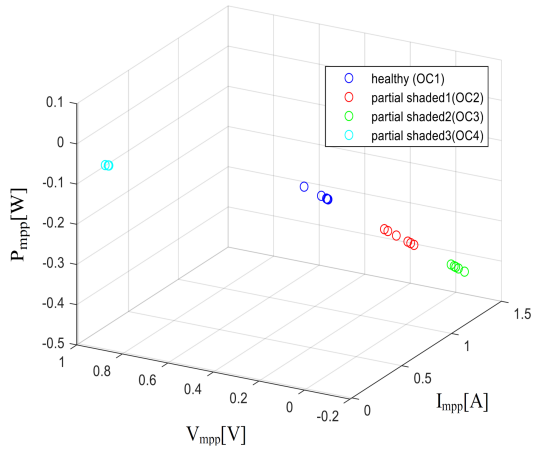

Fig. 13. Projection of the testing MPP coordinates dataset onto the CVA subspace.

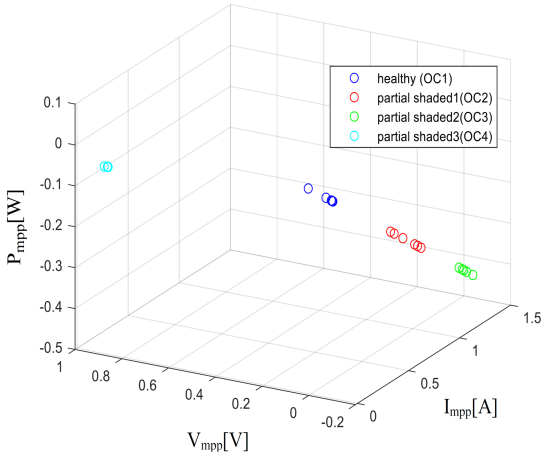

Fig. 14. Projection of the training MPP coordinates dataset onto the CVA subspace.

summarizes the main advantages and limitations of the diagnosis method proposed in this paper and the method developed in [28] using PCA.

3.2. Voltage estimation at MPP

In this paper, the voltage estimation at MPP was performed for PV panels operating on one STC and three different PSCs. When the system operates in PSC, it has a P–V curve with multiple peaks. SVR was used to determine the global MPP point and estimate the voltage at that point.

Although the support vector method was originally introduced as an algorithm for classification and support vector machines (SVM), it is also used in SVR regression problems. The difference between these two support vector methods is that while SVM labels the data, SVR continuously estimates the data value for the input data. In other words, while SVM operates on discrete data values, SVR operates on continuous data values. Support vector methods have high generalization performance

TABLE III

Overview of the proposed methods for detecting OC (partial shading) in PV systems.

Method	I–V Curve analysis (PCA) [28]	MPP analysis (CVA)
advantages	• sensitive to fault severity • suitable for small PV plants • adapted with online I–V tracer	• sensitive to fault severity • in terms of amount of observations used – cost effective – less memory storage • earlier fault detection allowing an optimized maintenance
limitations (for large scale PV plants)	• less plants convenient • additional cost with I–V tracer • sensitivity to I–V curve quality	• depending on the training dataset size and variety, it achieves efficient and accurate fault detection
used variables	• current, voltage, and power (I, V, P) • more observations for each variable	• current, voltage and power at MPP $(I_{\mathrm{MPP}}, V_{\mathrm{MPP}}, P_{\mathrm{MPP}})$ • observations only at MPP

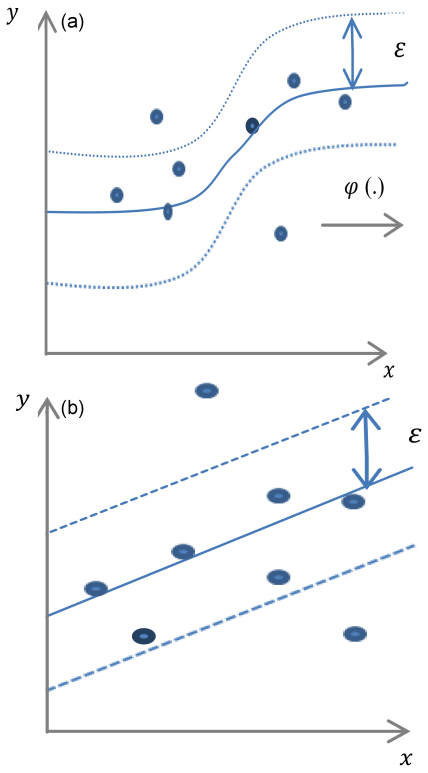

Fig. 15. Data transformation from (a) a nonlinear input space into (b) a linear higher dimensional space.

and are efficient in solving classification problems. The most prominent and important advantage of SVR methods is that they transform the classification/regression problem into a quadratic optimization problem and solve it. Thus, the number of operations for solving the problem in the learning phase is reduced, and a faster solution is achieved compared to other methods [29]. Due to this feature, these methods provide a great advantage, especially in large datasets. In addition, since support vector methods are optimization-based, they are more successful than other methods in terms of classification/regression performance, computational complexity, and usability [30].

The purpose of SVR analysis is to determine a mathematical function to accurately predict desired outputs ($\boldsymbol{y}_s in \mathrm{R}$) of a given dataset $\mathrm{D} = \{(x_s, y_s)| \in \{1, 2, \ldots, N\}$, where x_s are the inputs. Regression problems can be classified as linear and nonlinear regression problems. SVR was mainly developed for the solution of nonlinear regression problems. The SVR method transforms the training data from the input space to a higher dimensional space with the help of a nonlinear function in order to solve a nonlinear regression problem. Thus, a nonlinear problem in a lower dimension transforms into a linear problem in a higher dimension (Fig. 15).

Then, it applies linear regression in this high dimensional space. The mathematical representation of the obtained linear function to find the best regression is as follows

$$f(\boldsymbol{x}, \boldsymbol{w}) = b + \sum_{s=1}^{N} w_s \phi(x_s) + b = b + \boldsymbol{w}^{\mathrm{T}} \phi(\boldsymbol{x}), \tag{5}$$

where $\boldsymbol{w} \in \mathbb{R}^{\mathrm{m}}$ is the model parameter vector and $b \in \mathbb{R}$ is the vertical axis deviation term. Performing linear regression in high dimensional space, the objective function of SVR generally consists of minimizing ε-insensitive loss function L_ε and parameters representing the model. This is expressed by

$$\min J(\boldsymbol{w}, b) = \tfrac{1}{2} \sum_{s=1}^{N} |\boldsymbol{w}|^2 + C \sum_{s=1}^{N} L_\varepsilon\Big(y_s, f(x_s)\Big), \tag{6}$$

where $C \in \mathbb{R}^+$ is a constant.

In this paper, the instantly measured historical data of PV systems are used in order to perform the voltage estimation at MPP in case of a specified OC of the PV systems that operate on different OC, such as one STC and three different PSCs. The original data is partitioned into two as a training set and a test set since SVR is a supervised regression algorithm. The training dataset consists of data samples that have a 1×3 dimensional vector form containing I, V, and P values of a PV system. The voltage values at MPP are known for the data samples in the training set. The voltage estimation model is constructed using the training set.

TABLE IV

Comparative V_{MPP} estimation results of performance metrics.

Performance criteria	Proposed OCC based MPP estimation		SVR		ANN	
	MSE	RMSE	MSE	RMSE	MSE	RMSE
OC1	6.7470×10^{-5}	0.00824	0.1765	0.4200	0.00391	0.05886
OC2	2.3580×10^{-6}	0.00154	0.2155	0.4635	0.00504	0.05921
OC3	2.0747×10^{-5}	0.00458	0.3174	0.5624	0.00537	0.06383
OC4	1.6110×10^{-5}	0.00400	1.7694	1.3301	0.00286	0.05022

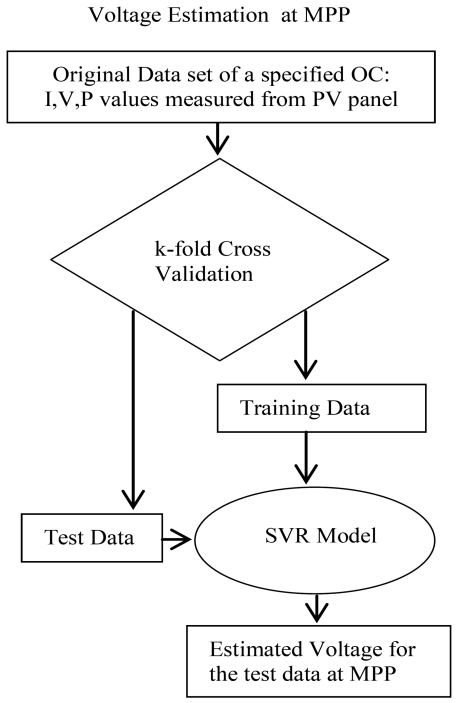

Fig. 16. The regression model construction step of the proposed MPP estimation method.

The test set consists of data samples that have the same form as the data samples in the training set, with only the MPP values not being exact. The voltage estimation at MPPs is performed by applying the test data sample to the constructed regression model. The flow chart of the proposed regression model is given in Fig. 16.

The error results of this voltage estimation at MPPs are obtained in terms of root mean squares (RMSE) and mean square error (MSE) and are given in Table IV.

The voltage estimation performance of the proposed method is compared with the voltage estimation performance of SVR and ANN. As the performance measure, indicators MSE and RMSE are used. The experimental results given in Table IV show that the proposed model yields MSE and RMSE that are better than those of the SVR and ANN models.

4. Conclusions

In this study, a novel customized MPPE method based on OCC that estimates the voltage at MPP for a PV system is proposed. In order to provide optimal performance for a PV system, the system must operate at MPP. Many method proposals can be found in the literature to find the MPP of a PV system. Since varying environmental factors cause changes in the OC of the PV panel, the power produced by the system also varies. There is only one peak in the P–V curve to the STC of the PV system, and that is the global MPP. However, multiple peaks occur in the P–V curve for a different OC, only one of which is the global MPP, while the others are the local MPPs. In this case, the OC has to be detected, and the method to find the MPP has to be customized in accordance with the varying OC. In this paper, a novel MPP estimation method based on OCC is proposed. The OCC is performed with CVA using historical data obtained over 18 min for each of the PV systems operating under different OC for different panel temperatures and different solar irradiation. Then, the voltage estimation at MPP is performed using the instantly measured historical data of the panel in the OCC. The OCC is performed with 100% accuracy in the proposed customization MPPE method that uses CVA, and the MPP estimation error rates are significantly reduced compared to the conventional methods used to find the MPP of the PV system.

References

[1] P.C. Chen, P.Y. Chen, Y.H. Liu, J.H. Chen, Y.F. Luo, *Sol. Energy.* **119**, 261 (2015).

[2] A.F. Paulo, G.S. Porto, *J. Clean. Prod.* **204**, 310 (2018).

[3] Y. Xie, T. Huang, J. Li, J. Liu, J. Niu, C.M. Mak, Z. Lin, *Build. Environ.* **132**, 45 (2018).

[4] A. Montecucco, A.R. Knox, *IEEE Trans. Power Electr.* **30**, 828 (2015).

[5] M. Metry, M.B. Shadmand, R.S. Balog, H. Abu-Rub, *IEEE Trans. Ind. Appl.* **53**, 1157 (2017).

[6] A. Ali, K. Almutairi, M.Z. Malik, K. Irshad, V. Tirth, S. Algarni, N.K. Shukla, *Energies* **13**, 3256 (2020).

[7] A.O. Baba, G. Liu, X. Chen, *Sustainable Futures* **2**, 100020 (2020).

[8] M.H. Zafar, N.M. Khan, A.F. Mirza, M. Mansoor, *J. Clean. Prod.* **309**, 127279 (2021).

[9] M.B. Smida, A. Sakly, S. Vaidyanathan, A.T. Azar, in: *Research Anthology on Clean Energy Management and Solutions*, IGI Global, 2021, p. 353.

[10] B. Kiriş, O. Bingöl, R. Şenol, A. Altintaş, *Acta Phys. Pol. A* **130**, 55 (2016).

[11] Z. Erdem, *Acta Phys. Pol. A* **132**, 1134 (2017).

[12] B. Subudhi, R. Pradhan, *IEEE Trans. Sustain. Energy* **4**, 89 (2012).

[13] K. Yan, Y. Du, Z. Ren, *IEEE Trans. Sustain. Energy* **10**, 2 (2018).

[14] Y. Du, X. Li, H. Wen, W. Xiao, in: *Proc. of the 2015 IEEE 16th Workshop on Control and Modelling for Power Electronics (COMPEL)*, Vancouver 2015.

[15] Y. Du, K. Yan, Z. Ren, W. Xiao, *Energies*, **11**, 10 (2018).

[16] S. Fadhel, D. Diallo, C. Delpha, A. Migan, I. Bahri, M. Trabelsi, M.F. Mimouni, *Energ. Convers. Manage.* **224**, 1 (2020).

[17] K. Yan, Z. Ji, H. Lu, J. Huang, W. Shen, Y. Xue, *IEEE Trans. Syst. Man Cybern. Syst.* **49**, 7 (2017).

[18] S. Pashiardis, S.A. Kalogirou, A. Pelengaris, *Appl. Energy* **190**, 1138 (2017).

[19] K. Yan, Z. Ji, W. Shen, *Neurocomputing* **228**, 205 (2017).

[20] J. Ma, H. Jiang, Z. Bi, K. Huang, X. Li, H. Wen, *IEEE T. Indust. Appl.* **55**, 1890 (2018).

[21] L. Bouselham, M. Hajji, B. Hajji, H. Bouali, *Energy Procedia* **111**, 924 (2017).

[22] U. Turhal, Y. Onal, *Acta Phys. Pol. A* **137**, 421 (2020).

[23] S.A. Rizzo, G. Scelba, *J. Clean. Prod.* **298**, 126775 (2021).

[24] Z. Erdem, *Acta Phys. Pol. A* **132**, 1128 (2017).

[25] E. Seke, Y. Anagün, N. Adar, *IET Image Process.* **12**, 2292 (2018).

[26] Z. Aytaç, N. Gülmezoğlu, M.B. Gülmezoğlu, *Int. J. Sustain. Agric. Manag. Inform.* **2**, 66 (2016).

[27] M. Yumurtaci, G. Gökmen, Ç. Kocaman, S. Ergin, O. Kilic, *Turkish J. Electr. Eng. Comput. Sci.* **24**, 1901 (2016).

[28] S. Fadhel, C. Delpha, D. Diallo, I. Bahri, A. Migan, M. Trabelsi, M.F. Mimouni, *Solar Energy* **179**, 1 (2019).

[29] E.A. Mahareek, A.S. Desuky, H.A. El-Zhni *Bull. Electr. Eng. Inform.* **10**, 1211 (2021).

[30] M. Singla, D. Ghosh, K.K. Shukla, *Int. J. Mach. Learn. Cybern.* **11**, 1359 (2020).